Technical University of Denmark

DTU

Increasing the blue-shift of a supercontinuum by modifying the fiber glass composition

Frosz, Michael Henoch; Moselund, Peter M.; Rasmussen, Per Dalgaard; Thomsen, Carsten L.; Bang, Ole

Link back to DTU Orbit

DTU Library
Technical Information Center of Denmark

Increasing the blue-shift of a supercontinuum by modifying the fiber glass composition

Michael H. Frosz[1,2], Peter M. Moselund[1,2], Per D. Rasmussen[1], Carsten L. Thomsen[2], Ole Bang[1]

[1]*DTU Fotonik, Department of Photonics Engineering, Technical University of Denmark, Ørsteds Plads 343, DK-2800 Kgs. Lyngby, Denmark*
[2]*Koheras A/S, Blokken 84, DK-3460 Birkerød, Denmark*
mhfr@fotonik.dtu.dk

http://www.fotonik.dtu.dk

Abstract: Supercontinuum light sources spanning into the ultraviolet–visible wavelength region are highly useful for applications such as fluorescence microscopy. A method of shifting the supercontinuum spectrum into this wavelength region has recently become well understood. The method relies on designing the group-velocity profile of the nonlinear fiber in which the supercontinuum is generated, so that red-shifted solitons are group-velocity matched to dispersive waves in the desired ultraviolet-visible wavelength region. The group-velocity profile of a photonic crystal fiber (PCF) can be engineered through the structure of the PCF, but this mostly modifies the group-velocity in the long-wavelength part of the spectrum. In this work, we first consider how the group-velocity profile can be engineered more directly in the short-wavelength part of the spectrum through alternative choices of the glass material from which the PCF is made. We then make simulations of supercontinuum generation in PCFs made of alternative glass materials. It is found that it is possible to increase the blue-shift of the generated supercontinuum by about 20 nm through a careful choice of glass composition, provided that the alternative glass composition does not have a significantly higher loss than silica in the near-infrared.

References and links

1. J. K. Ranka, R. S. Windeler, and A. J. Stentz, "Visible continuum generation in air-silica microstructure optical fibers with anomalous dispersion at 800 nm," Opt. Lett. **25**, 25–27 (2000).
2. M.-C. Chan, S.-H. Chia, T.-M. Liu, T.-H. Tsai, M.-C. Ho, A. Ivanov, A. Zheltikov, J.-Y. Liu, H.-L. Liu, and C.-K. Sun, "1.2- to 2.2-μm Tunable Raman Soliton Source Based on a Cr:Forsterite Laser and a Photonic-Crystal Fiber," IEEE Photon. Technol. Lett. **20**, 900–902 (2008).
3. J. Walewski, M. Borden, and S. Sanders, "Wavelength-agile laser system based on soliton self-shift and its application for broadband spectroscopy," Appl. Phys. B. **79**, 937–940 (2004).

4. E. R. Andresen, C. K. Nielsen, J. Thøgersen, and S. R. Keiding, "Fiber laser-based light source for coherent anti-Stokes Raman scattering microspectroscopy," Opt. Express **15**, 4848–4856 (2007). URL http://www.opticsexpress.org/abstract.cfm?URI=oe-15-8-4848.

5. C. Xia, M. Kumar, O. P. Kulkarni, M. N. Islam, J. Fred L. Terry, M. J. Freeman, M. Poulain, and G. Mazé, "Mid-infrared supercontinuum generation to 4.5 μm in ZBLAN fluoride fibers by nanosecond diode pumping," Opt. Lett. **31**, 2553–2555 (2006). URL http://ol.osa.org/abstract.cfm?URI=ol-31-17-2553.

6. P. N. Prasad, *Introduction to biophotonics* (John Wiley & Sons Inc., 2003).

7. http://www.koheras.com/.

8. K. Jalink, A. Diaspro, V. Caorsi, and P. Bianchini, "Leica TCS SP5 X – White Light Laser," Application Letter 29, Leica Microsystems (2008). http://www.leica-microsystems.com.

9. A. Kudlinski, A. K. George, J. C. Knight, J. C. Travers, A. B. Rulkov, S. V. Popov, and J. R. Taylor, "Zero-dispersion wavelength decreasing photonic crystal fibers for ultraviolet-extended supercontinuum generation," Opt. Express **14**, 5715–5722 (2006). URL http://www.opticsexpress.org/abstract.cfm?URI=oe-14-12-5715.

10. F. Lu, Y. Deng, and W. H. Knox, "Generation of broadband femtosecond visible pulses in dispersion-micromanaged holey fibers," Opt. Lett. **30**, 1566–1568 (2005). http://www.opticsinfobase.org/abstract.cfm?URI=ol-30-12-1566.

11. P. Westbrook, J. Nicholson, K. Feder, Y. Li, and T. Brown, "Supercontinuum generation in a fiber grating," Appl. Phys. Lett. **85**, 4600–4602 (2004).

12. J. A. Bolger, F. Luan, D.-I. Yeom, E. N. Tsoy, C. M. de Sterke, and B. J. Eggleton, "Tunable enhancement of a soliton spectrum using an acoustic long-period grating," Opt. Express **15**, 13,457–13,462 (2007). URL http://www.opticsexpress.org/abstract.cfm?URI=oe-15-20-13457.

13. N. I. Nikolov, T. Sørensen, O. Bang, and A. Bjarklev, "Improving efficiency of supercontinuum generation in photonic crystal fibers by direct degenerate four-wave mixing," J. Opt. Soc. Am. B **20**, 2329–2337 (2003).

14. M. H. Frosz, T. Sørensen, and O. Bang, "Nanoengineering of photonic crystal fibers for supercontinuum spectral shaping," J. Opt. Soc. Am. B **23**, 1692–1699 (2006). http://www.opticsinfobase.org/abstract.cfm?URI=josab-23-8-1692.

15. P. M. Moselund, M. H. Frosz, C. L. Thomsen, and O. Bang, "Back-seeding of higher order gain processes in picosecond supercontinuum generation," Opt. Express **16**, 11,954–11,968 (2008). URL http://www.opticsexpress.org/abstract.cfm?URI=oe-16-16-11954.

16. J. M. Stone and J. C. Knight, "Visibly "white" light generation in uniform photonic crystal fiber using a microchip laser," Opt. Express **16**, 2670–2675 (2008). URL http://www.opticsexpress.org/abstract.cfm?URI=oe-16-4-2670.

17. L. Tartara, I. Cristiani, and V. Degiorgio, "Blue light and infrared continuum generation by soliton fission in a microstructured fiber," Appl. Phys. B. **77**, 307 (2003).

18. J. M. Dudley, G. Genty, and S. Coen, "Supercontinuum generation in photonic crystal fiber," Rev. Mod. Phys. **78**, 1135–1184 (2006). http://link.aps.org/abstract/RMP/v78/p1135.

19. G. P. Agrawal, *Nonlinear Fiber Optics*, 4th ed. (Academic Press, Burlington, MA, USA, 2007).

20. G. Genty, M. Lehtonen, and H. Ludvigsen, "Effect of cross-phase modulation on supercontinuum generated in microstructured fibers with sub-30 fs pulses," Opt. Express **12**, 4614–4624 (2004). http://www.opticsexpress.org/abstract.cfm?URI=OPEX-12-19-4614.

21. G. Genty, M. Lehtonen, and H. Ludvigsen, "Route to broadband blue-light generation in microstructured fibers," Opt. Lett. **30**, 756–758 (2005). URL http://ol.osa.org/abstract.cfm?URI=ol-30-7-756.

22. A. V. Gorbach, D. V. Skryabin, J. M. Stone, and J. C. Knight, "Four-wave mixing of solitons with radiation and quasi-nondispersive wave packets at the short-wavelength edge of a supercontinuum," Opt. Express **14**, 9854–9863 (2006). URL http://www.opticsexpress.org/abstract.cfm?URI=oe-14-21-9854.

23. N. Nishizawa and T. Goto, "Characteristics of pulse trapping by ultrashort soliton pulses in optical fibers across the zero-dispersion wavelength," Opt. Express **10**, 1151–1160 (2002). URL http://www.opticsexpress.org/abstract.cfm?URI=oe-10-21-1151.

24. A. V. Gorbach and D. V. Skryabin, "Light trapping in gravity-like potentials and expansion of supercontinuum spectra in photonic-crystal fibres," Nature Photonics **1**, 653–657 (2007).

25. D. V. Skryabin, F. Luan, J. C. Knight, and P. S. J. Russell, "Soliton self-frequency shift cancellation in photonic crystal fibers," Science **301**, 1705–1708 (2003).

26. J. C. Travers, S. V. Popov, and J. R. Taylor, "Trapping of dispersive waves by solitons in long lengths of tapered PCF," 2008 Conference on Lasers and Electro-Optics and 2008 Conference on Quantum Electronics and Laser Science pp. 1–2 (2008).

27. J. C. Travers, A. B. Rulkov, B. A. Cumberland, S. V. Popov, and J. R. Taylor, "Visible supercontinuum generation in photonic crystal fibers with a 400 W continuous wave fiber laser," Opt. Express **16**, 14,435–14,447 (2008). URL http://www.opticsexpress.org/abstract.cfm?URI=oe-16-19-14435.

28. P. Leproux, C. Buy-Lesvigne, V. Tombelaine, V. Couderc, J. Auguste, J. Blondy, G. Mélin, K. Schuster, J. Kobelke, and H. Bartelt, "Methods for visible supercontinuum generation in doped/undoped holey fibres," Proceedings of the SPIE - The International Society for Optical Engineering **6990**, 699,007–1–4 (2008).

29. V. Tombelaine, C. Buy-Lesvigne, V. Couderc, P. Leproux, G. Mélin, K. Schuster, J. Kobelke, and H. Bartelt, "Second harmonic generation in Ge-doped silica holey fibres and supercontinuum generation," Proceedings of

the SPIE - The International Society for Optical Engineering **6990**, 69,900N–1–7 (2008a).

30. V. Tombelaine, C. Buy-Lesvigne, P. Leproux, V. Couderc, and G. Mélin, "Optical poling in germanium-doped microstructured optical fiber for visible supercontinuum generation," Opt. Lett. **33**, 2011–2013 (2008b). URL http://ol.osa.org/abstract.cfm?URI=ol-33-17-2011.

31. J. W. Fleming, "Material dispersion in lightguide glasses," Electron. Lett. **14**, 326–8 (1978).

32. J. W. Fleming, "Material dispersion in lightguide glasses [Erratum]," Electron. Lett. **15**, 507 (1979).

33. I. H. Malitson, "Interspecimen comparison of the refractive index of fused silica," Journal of the Optical Society of America **55**, 1205–1209 (1965).

34. COMSOL Multiphysics 3.4 (2007). http://www.comsol.com.

35. P. V. Mamyshev and S. V. Chernikov, "Ultrashort-pulse propagation in optical fibers," Opt. Lett. **15**, 1076–1078 (1990).

36. J. Lægsgaard, "Mode profile dispersion in the generalised nonlinear Schrödinger equation," Opt. Express **15**, 16 110–16123 (2007).

37. K. J. Blow and D. Wood, "Theoretical description of transient stimulated Raman scattering in optical fibers," IEEE J. Quantum Electron. **25**, 2665–2673 (1989).

38. S. Kobayashi, N. Shibata, S. Shibata, and T. Izawa, "Characteristics of optical fibers in infrared wavelength region," Review of the Electrical Communication Laboratories **26**, 453–67 (1978).

39. O. V. Sinkin, R. Holzlöhner, J. Zweck, and C. R. Menyuk, "Optimization of the Split-Step Fourier Method in Modeling Optical-Fiber Communications Systems," J. Lightwave Technol. **21**, 61–68 (2003). http://dx.doi.org/10.1109/JLT.2003.808628.

40. M. H. Frosz, O. Bang, and A. Bjarklev, "Soliton collision and Raman gain regimes in continuous-wave pumped supercontinuum generation," Opt. Express **14**, 9391–9407 (2006). http://www.opticsinfobase.org/abstract.cfm?URI=oe-14-20-9391.

41. S. B. Cavalcanti, G. P. Agrawal, and M. Yu, "Noise amplification in dispersive nonlinear media," Phys. Rev. A **51**, 4086–4092 (1995). http://dx.doi.org/10.1103/PhysRevA.51.4086.

42. A. Mussot, E. Lantz, H. Maillotte, T. Sylvestre, C. Finot, and S. Pitois, "Spectral broadening of a partially coherent CW laser beam in single-mode optical fibers," Opt. Express **12**, 2838–2843 (2004). http://www.opticsexpress.org/abstract.cfm?URI=OPEX-12-13-2838.

43. T. Kato, Y. Suetsugu, and M. Nishimura, "Estimation of nonlinear refractive index in various silica-based glasses for optical fibers," Opt. Lett. **20**, 2279 (1995). URL http://ol.osa.org/abstract.cfm?URI=ol-20-22-2279.

44. W. H. Press, S. A. Teukolsky, W. T. Vetterling, and B. P. Flannery, *Numerical Recipes in C++: The Art of Scientific Computing*, 2nd ed. (Cambridge University Press, Cambridge, 2002). http://www.nr.com.

1. Introduction

The first experiments with supercontinuum generation in a photonic crystal fibre (PCF) demonstrated impressive spectra spanning from 400 nm to 1500 nm using 100 fs pulses [1]. Often, one does not require the use of the entire supercontinuum bandwidth, or the spectrum needs to be concentrated in a specific spectral region where other lasers are not readily available. To achieve spectral energy at wavelengths longer than provided by a given pump laser, one can use the soliton self-frequency shift to simply red-shift the laser pulse over a desired wavelength range. This can be done over 900 nm [2] and provides a basis for tunable lasers with applications including broadband spectroscopy [3] and coherent anti-Stokes Raman scattering (CARS) microspectroscopy [4]. ZBLAN fluoride (a mixture of zirconium, barium, lanthanum, aluminum, and sodium fluorides) fibres have been used to extend the supercontinuum spectrum beyond 4.5 μm [5]. Besides these examples of generating light in the near- or mid-infrared, one also finds examples of generating light in the ultraviolet–blue region of the spectrum. This wavelength region is highly interesting for several reasons. Primarily, many fluorescent molecules are excited in a wavelength range from ∼600 nm down to ∼350 nm [6]. Supercontinuum light sources covering this wavelength range are therefore highly useful for fluorescence microscopy. In particular, a high power spectral density over a broad wavelength range removes the need for using several lasers, each corresponding to the excitation wavelength of a specific fluorescent molecule. Supercontinuum sources with high spectral density between 460 nm and 2400 nm have now become commercially available [7]. Such supercontinuum sources are, e.g., the essential building block in state-of-the-art supercontinuum confocal microscopy systems, allowing continuous tuning of the excitation wavelength [8]. Another application is absorption

spectroscopy in the ultraviolet–visible region.

Due to the complexity of supercontinuum generation in general, there is more than one way of achieving significant spectral power in the ultraviolet–visible region of the spectrum. Continuously shifting the zero-dispersion wavelength (ZDW) along a fiber by tapering it, has been used to generate light in the UV-visible region both using ns–ps long pulses [9] and fs pulses [10]. Concerning enhancement of the supercontinuum in the near-infrared, it has been demonstrated that the supercontinuum can be enhanced near the Bragg resonance wavelength of a fiber Bragg grating [11]. This principle was also demonstrated for a tunable acoustic long-period grating [12]. Another basic approach for controlling the supercontinuum spectrum is through careful dispersion engineering of a PCF. This can be used to control the location of the Stokes and anti-Stokes peaks in a ps-pumped supercontinuum dominated by four-wave mixing (FWM) [13, 14]. The FWM peaks can also be locally enhanced by back-seeding part of the supercontinuum [15]. Dispersion engineering can also be done as post-processing through UV-irradiation of germano-silicate fibers, which has been used to extend the blue-shift of the supercontinuum [**?**].

In this paper we focus on a particular route for generating spectral power in the UV-visible region. This particular route has become well understood and is based on group-velocity matching between red-shifting solitons and dispersive waves blue-shifted by the interaction with the solitons [17, 20, 21, 22, 24]. We investigate to what extent one can increase the blue-shift of a supercontinuum, by changing the group-velocity profile through the use of fibre materials other than pure silica. The group-velocity profile has previously been manipulated for increased blue-shift by changing the PCF structure [16]. However, this primarily modifies the group-velocity for longer wavelengths. Our approach here is to manipulate the group-velocity profile for shorter wavelengths by changing the glass composition of the fiber. The spectral broadening mechanism is explained in detail in Section 2, where we also discuss how the group-velocity profile should be modified for increased blue-shift. In Section 3 we calculate the group-velocity profiles of various glass compositions. Section 4 describes how we then simulate supercontinuum generation in fibres made of these glasses. The results of the simulations are presented and discussed in Section 5. Finally, in Section 6 we conclude this paper.

2. Theory

The method investigated here for blue-shifting the supercontinuum consists of first breaking the pump pulses up into short ($\lesssim$ 100 fs) red-shifting solitons, while the solitons generate dispersive waves in the normal dispersion region on the short-wavelength side of the pump. This can be achieved by pumping at a wavelength with anomalous dispersion but close to the ZDW of the PCF [18, 19]. Assuming that the dispersive waves initially have a lower group-velocity than the solitons, they will lag behind the solitons. However, as the solitons gradually red-shift they will also experience a reduction in group-velocity and eventually meet with the dispersive waves. The temporal overlap between a soliton and a dispersive wave allows them to interact nonlinearly. Two mechanisms have been suggested for this interaction. First, the temporal overlap with the high power soliton leads to cross-phase modulation (XPM) [19] of the dispersive wave. Since the dispersive wave is located on the trailing edge of the soliton, the XPM leads to a blue-shift of the dispersive wave [20, 21]. Second, a type of four-wave mixing (FWM) can occur between the soliton and the dispersive wave which leads to the generation of energy at wavelengths shorter than the dispersive wave [22]. For both of the two methods, the blue-shifted radiation experiences a decrease in group-velocity and will therefore lag behind the soliton. But as long as the soliton can continue its red-shift, it will also decrease its group-velocity until it again meets with the blue-shifted radiation. The blue-shift mechanism can therefore take place continuously, as long as the soliton is able to red-shift and decrease its group-velocity (note that
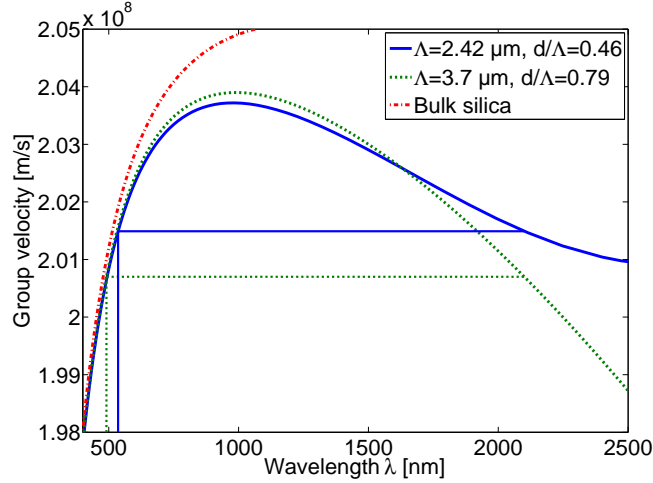
Fig. 1. Calculated group-velocity profiles for PCFs with $\Lambda = 2.42$ µm, $d/\Lambda = 0.46$ (blue, solid) and $\Lambda = 3.7$ µm, $d/\Lambda = 0.79$ (green, dotted). The horizontal and vertical lines show that there is group-velocity match from 2100 nm to 536 nm in the $\Lambda = 2.42$ µm, $d/\Lambda = 0.46$ fibre, while the $\Lambda = 3.7$ µm, $d/\Lambda = 0.79$ provides group-velocity match from 2100 nm to 491 nm. The group-velocity in bulk silica is also indicated (red, dash-dotted).

solitons only exist in the anomalous dispersion region, where a red-shift implies a decrease in group-velocity). Since the blue-shifted radiation cannot escape from the soliton as long as this cycle continues, this process has also been termed a "trapping effect" [23, 24]. A first tentative explanation of this supercontinuum blue-shift mechanism was given by Tartara *et al.* [17]. Recently, the explanation has been firmly experimentally supported in the work by Stone *et al.* [16]. With this mechanism the maximum blue-shift is limited by the ability of the solitons to red-shift. The red-shift can be limited by the increase in both material loss and confinement loss for wavelengths in the near-infrared. Depending on the structural design of the PCF, the existence of a second ZDW will also limit the soliton red-shift, since the red-shift is halted gradually by spectral recoil as the solitons red-shift to the vicinity of the second ZDW [25].

More directly, the maximum blue-shift is also determined by the group-velocity profile: the group-velocity of the most red-shifted solitons matches the group-velocity of the most blue-shifted dispersive wave [22, 24, 27]. One could therefore manipulate the group-velocity profile through careful PCF design to increase the blue-shift. The work by Stone *et al.* focused on modifying the PCF structure so that the group-velocities were lowered for the red-shifting solitons [16]. The principle of this is demonstrated in Fig. 1. In this figure, it is seen that for a PCF with the structural parameters $\Lambda = 2.42$ µm, $d/\Lambda = 0.46$ a soliton red-shifted to 2100 nm is group-velocity matched to a dispersive wave at 536 nm (we neglect the nonlinear contribution to the group-velocity of a soliton, since it is small compared to the linear group-velocity). Instead choosing a PCF with $\Lambda = 3.7$ µm, $d/\Lambda = 0.79$ shifts the group-velocity match to 491 nm for a soliton with the same red-shift. This means that a larger blue-shift can be expected in a supercontinuum generated in the PCF with $\Lambda = 3.7$ µm, $d/\Lambda = 0.79$. Note that the PCF group-velocity profiles below ~700 nm are practically equal, since material dispersion is dominant for short wavelengths, while waveguide dispersion becomes more dominant for long wavelengths. It is also indicated in the figure how the PCF group-velocity profiles approach the group-velocity of bulk silica at short wavelengths.

If one wishes to carefully design the PCF group-velocity profile for increased blue-shift of
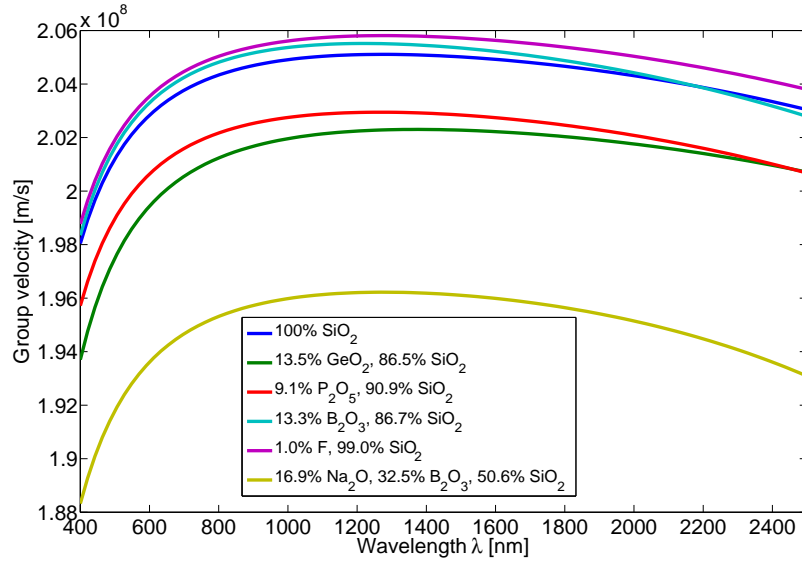
Fig. 2. Calculated group velocity profiles for 6 different glass compositions, including pure silica.

the supercontinuum, it is clear from the above considerations that changing the PCF structural parameters will primarily modify the group-velocity profile for long wavelengths. Furthermore, modifying the PCF structure in order to lower the group-velocities for long wavelengths can shift the zero-dispersion wavelength (ZDW) away from the desired pump wavelength, thereby reducing the amount of power transferred to the UV–visible region [16].

An alternative approach is to change the group-velocity profile by choosing a fibre material different from pure silica. The group-velocity profile is then no longer restricted to always approach the group-velocity of silica at shorter wavelengths. This approach therefore expands the possibilities for dispersion design of PCFs.

We should also mention that experiments of visible supercontinuum generation in Ge-doped fibres were recently presented [28, 29, 30] but the objective of the doping was to increase the second-harmonic generation in the fibre, and not to modify the group-velocity profile.

3. Modifying the group-velocity profile by modifying the glass composition

It was explained in Section 2 that shifting the group-velocity profile downwards for the long-wavelength part of the spectrum leads to an increased blue-shift. This is because the red-shifting solitons are then able to match the group-velocity of dispersive waves at shorter wavelengths. Likewise, upshifting the group-velocity profile $v_g(\lambda)$ for the short-wavelength part of the spectrum should also lead to an increased blue-shift of the supercontinuum. To investigate whether a suitable manipulation of the short-wavelength part of the group-velocity profile is possible by modifying the glass composition from which the fibre is drawn, we calculated $v_g(\lambda)$ for a range of characteristic compositions of materials previously used in waveguides. The Sellmeier coefficients for the various glass compositions were obtained from Ref. [31, 32]; for pure fused silica we used the data from Ref. [33], which is used widely [19].

Figure 2 shows the calculated group-velocity profiles for 6 different bulk glass compositions, including pure silica. It is seen that out of the 5 alternative glass compositions investigated here, only two have a higher $v_g(\lambda)$ than silica in the visible part of the spectrum: 1.0% F and 13.3%
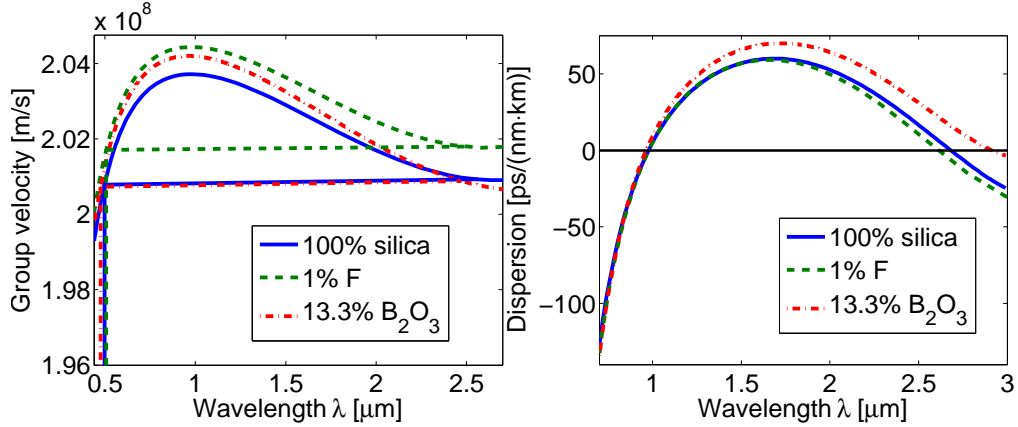
Fig. 3. *Left:* Calculated group-velocity profiles for a particular PCF structure ($\Lambda = 2.42$ μm, $d/\Lambda = 0.46$) of different glass compositions: pure fused silica (blue, solid line), 1% F (green, dashed), and 13.3% B_2O_3 (red, dash-dot). The vertical lines indicate the calculated location of the short-wavelength peak of the corresponding spectra (Fig. 5). From the intersections between these lines and the corresponding group velocities, a line has been drawn to the group-velocity at which the most red-shifted soliton is located. The line is practically horizontal, which shows that there is group-velocity match between the short-wavelength peak and the most red-shifted soliton. *Right:* Dispersion profiles corresponding to the same PCF structure and glass compositions. The black horizontal line indicates zero dispersion.

B_2O_3. We therefore continue investigating these two glass compositions.

The properties of the fundamental mode of a particular PCF ($\Lambda = 2.42$ μm, $d/\Lambda = 0.46$) made of these two alternative glass compositions were calculated using a mode solver based on the finite element method [34]. To investigate whether the change in glass composition changes the modal properties of the PCF (more specifically how the cut-off wavelength is affected), we calculated the effective V-parameter applicable for PCFs. It has been shown that PCFs are single-moded for $V_{eff} < \pi$ [?]. From this we found that the cut-off wavelength is about 492 nm for the pure silica PCF and shifts only slightly to about 486 nm for the alternative glass compositions. In Fig. 3 we show the resulting calculated group-velocity and dispersion profiles. It is seen in Fig. 3 (left) that choosing the glass with 1% F upshifts the entire group-velocity profile with a diminishing shift towards shorter wavelengths. The glass composition with 13.3% B_2O_3 results in a smaller upshift of $v_g(\lambda)$, and from a wavelength of approximately 2.3 μm and upwards the group velocity is smaller than for a pure silica fibre. Also, the glass with 13.3% B_2O_3 shifts the ZDW further into the near-infrared. Based on the understanding of the physical mechanism behind the short-wavelength part of the spectrum, presented in Section 2, we can now use the group-velocity profiles to make the following predictions about the short-wavelength edge of supercontinua generated in the three fibres investigated here.

One could initially think that the upshift of $v_g(\lambda)$ at short wavelengths for the fibre with 1% F would lead to a larger blue-shift. However, since $v_g(\lambda)$ is also shifted upwards for longer wavelengths, the red-shifting solitons are not expected to be able to slow down sufficiently to match their group-velocity to radiation at shorter wavelengths than in the pure silica fibre. On the other hand, red-shifting solitons in the 13.3% B_2O_3 fibre eventually experience a lower group-velocity than in the pure silica fibre, and are thus able to match their group-velocity to radiation at shorter wavelengths than in the pure silica fiber. From these considerations we expect that even though using glass with 1% F upshifts the group-velocity at the short-wavelength part

of the spectrum, this will not result in an increased blue-shift of the spectrum. Instead, using glass with 13.3% B_2O_3 is expected to result in a larger blue-shift.

In the following, we use numerical simulations of supercontinuum generation to test these expectations.

4. Propagation equation

The propagation of optical pulses in a nonlinear waveguide is often modelled using the generalized nonlinear Schrödinger equation (GNLSE). The GNLSE was recently reformulated to account for a strong frequency dependence of the effective area $A_{\text{eff}}(\omega)$ [35, 36]. This modified GNLSE is written here in a form very similar to the standard GNLSE:

$$\frac{\partial \tilde{C}}{\partial z} = i \sum_{m=2}^{\infty} \beta_m \frac{[\omega - \omega_0]^m}{m!} \tilde{C}(z, \omega) - \frac{\alpha(\omega)}{2} \tilde{C}(z, \omega)$$
$$+ i\gamma(\omega) \left[1 + \frac{\omega - \omega_0}{\omega_0} \right] \mathscr{F} \left\{ C(z,t) \int_{-\infty}^{\infty} R(t - t_1) |C(z,t)|^2 \, dt_1 \right\}, \tag{1}$$

where the nonlinear coefficient $\gamma(\omega)$ is given by

$$\gamma(\omega) = \frac{n_2 n_0 \omega_0}{c n_{\text{eff}}(\omega) \sqrt{A_{\text{eff}}(\omega) A_{\text{eff}}(\omega_0)}}. \tag{2}$$

n_2 is the nonlinear-index coefficient of the waveguide material set to the value corresponding to fused silica: $n_2 = 2.6 \cdot 10^{-20}$ m^2/W [19]. $n_{\text{eff}}(\omega)$ is the frequency dependent effective index of the guided mode and $n_0 = n_{\text{eff}}(\omega_0)$. The variation of $n_{\text{eff}}(\omega)$ is usually much smaller than the variation of $A_{\text{eff}}(\omega)$ and therefore neglected here. $\tilde{C}(z, \omega)$ is the Fourier transform of $C(z,t)$, and is related to the Fourier transform of the pulse envelope $A(z,t)$ by

$$\tilde{C}(z, \omega) = \left[\frac{A_{\text{eff}}(\omega)}{A_{\text{eff}}(\omega_0)} \right]^{-1/4} \tilde{A}(z, \omega). \tag{3}$$

The symbol $\mathscr{F}$ denotes Fourier transform, and $R(t)$ is the Raman response of the nonlinear waveguide. For this work the standard approximation for silica glass was used [37, 19]:

$$R(t) = (1 - f_R)\delta(t) + f_R \frac{\tau_1^2 + \tau_2^2}{\tau_1 \tau_2^2} \exp(-t/\tau_2) \sin(t/\tau_1) \Theta(t), \tag{4}$$

where $\delta(t)$ is the Dirac delta function, $f_R = 0.18$ is the fractional Raman response, $\tau_1 = 12.2$ fs, $\tau_2 = 32$ fs, and $\Theta(t)$ is the Heaviside step function.

Note that Eq. (1) is reduced to the standard GNLSE [18, 19] if (1) C and $\tilde{C}$ are replaced by A and $\tilde{A}$, respectively, and if (2) $\gamma(\omega)$ is approximated by

$$\gamma(\omega) \approx \gamma(\omega_0) = \frac{n_2 \omega_0}{c A_{\text{eff}}(\omega_0)}. \tag{5}$$

This means that current implementations of numerical solutions to the standard GNLSE only need small modifications to instead solve the modified GNLSE, Eq. (1). A simple approach to include the frequency dependence of A_{eff}, has previously been to simply use the standard GNLSE, with a frequency dependent nonlinear coefficient given by

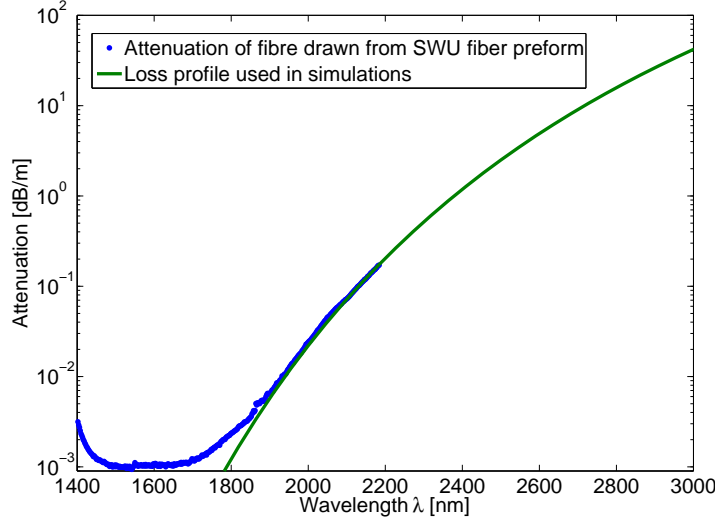$$\gamma(\omega) = \frac{n_2 \omega_0}{c A_{\text{eff}}(\omega)}. \tag{6}$$

Fig. 4. Measured loss in fibre drawn from all-silica step-index preform with F-doped cladding, used for optical fibers (blue dots), and the fitted loss profile used in the simulations (green line). Measured loss data kindly provided by Heraeus Quarzglas, Germany.

However, the modified GNLSE was recently found to more accurately take into account the wavelength dependence of A_{eff} than the simple approach [36].

$\alpha(\omega)$ in Eqn. (1) is the power attenuation coefficient. Losses in the near-infrared can be expected to limit the soliton red-shift. We have therefore included losses in the near-infrared region. The measured loss profile for an all-silica fibre is shown in Fig. 4. For the fibre lengths modelled here, the losses below $\sim$2000 nm are considered insignificant (the loss is below 0.1 dB/m in the range 420–2130 nm); we have therefore made a fit to the data between 2000–2184 nm. The loss in this wavelength range is dominated by the so-called multiphonon edge, seen as an absorption tail in the near-infrared. The losses above 2184 nm are calculated from extrapolation of the fit following the form $\alpha(\lambda) = A\exp(-a/\lambda)$. We could not find available data for the near-infrared loss profile of silica with 1% F or 13.3% B_2O_3, but the doping is expected to lead to an increased loss [38]. We therefore use the loss profile of pure silica in all the simulations with loss, and thus our investigation focuses on the effect of modifying the group-velocity profile through doping, without considering changes in loss due to the doping.

5. Simulation results

All the simulations were made with 2^{17} sampling points. The temporal resolution was set to 1.54 fs, resulting in a temporal window of 201.85 ps and a frequency resolution of 4.95 GHz. The simulations were made both with and without the loss profile of pure silica, because the numerical accuracy can better be evaluated when loss is not included. The adaptive step size method was used [39] with a local goal error of $\delta_G = 10^{-6}$ resulting in a maximum change in photon number (a measure of the numerical error which is ideally zero in the absence of loss) [36, 37] of $-5.9 \cdot 10^{-6}$% after 2.5 m of propagation for the simulations without loss. For validation, loss-free simulations were also performed up to a length of 0.25 m with $\delta_G = 10^{-8}$ resulting in a maximum change in photon number of $-5.0 \cdot 10^{-8}$%; the resulting spectra showed insignificant differences compared to the spectra using $\delta_G = 10^{-6}$, which at this length had a maximum change in photon number of $-4.5 \cdot 10^{-6}$%. Since the change in photon number is larger from $z = 0$ m to $z = 0.25$ m than from $z = 0.25$ m to $z = 2.5$ m and there was no
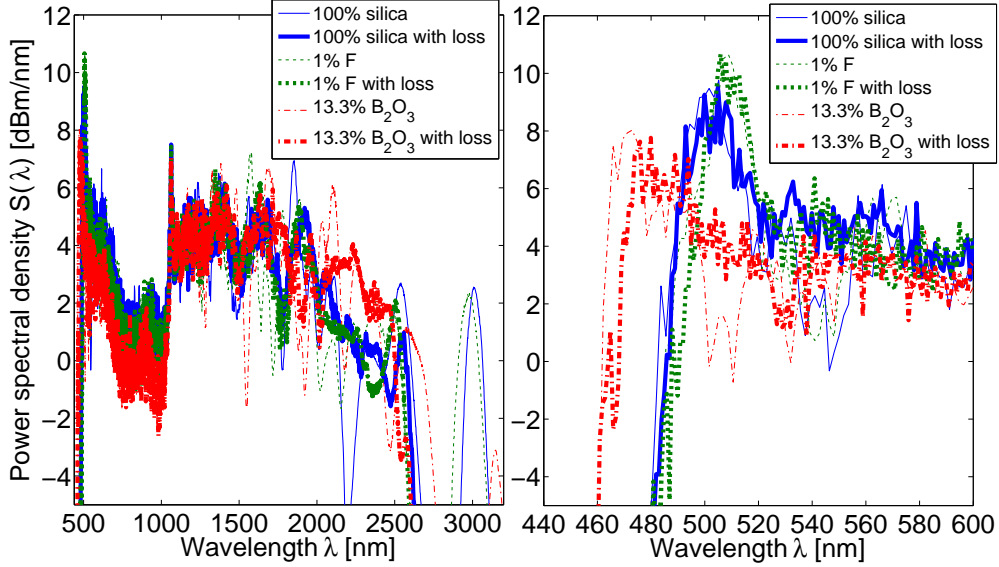
Fig. 5. Calculated spectra after 2.5 m of propagation in a PCF ($\Lambda = 2.42$ μm and $d/\Lambda = 0.46$) made of pure silica and alternative glass compositions. The spectra have been smoothed using Savitzky-Golay filtering [44]; the simulations including loss were first averaged over 5 simulations with different input noise seed for each glass composition.

significant difference in the spectra calculated with either $\delta_G = 10^{-6}$ or $\delta_G = 10^{-8}$ at 0.25 m, the numerical accuracy is assumed to be sufficient. The input pulse has a sech shape, peak power of 9 kW, intensity FWHM (full-width at half-maximum) duration of 8 ps, and centre wavelength of 1064 nm. To realistically model the finite linewidth of the pump laser, we used the same phase noise model as in Ref. [40], since the underlying phase-diffusion model is physically well-founded [41, 42]. The linewidth in the simulations was set to 530 GHz ($\sim$2 nm) FWHM. For each of the three glass compositions we made 5 simulations including loss and one without loss. The 5 simulations including loss were made using different initial seeds for the pseudo random number generator used for the phase noise. Since the spectral broadening is initiated by modulation instability, the final spectra are highly sensitive to the input noise [18]. It is therefore necessary to perform multiple simulations and average over the resulting spectra. In our case we found that 5 simulations were sufficient to get a reasonable averaging.

The centre wavelength of the simulation frequency window was set to 750 nm. The power spectra $S(\lambda)$ shown are scaled so that $\int_{\lambda_{min}}^{\lambda_{max}} S(\lambda)d\lambda$ is equal to the average pulse power, assuming a pulse repetition frequency of 80 MHz. To focus on the effect of changing the group-velocity profile by modifying the fibre material, we use the same loss profile for pure silica in all simulations with loss. Also, we have not considered how the nonlinearity of the material could be modified due to the alternative glass compositions (doping SiO_2 with either GeO_2 or F is known to increase n_2 [43]; a higher n_2 means that shorter fibers can be used to obtain a similar spectral broadening). Also, we have used $A_{eff}(\omega)$ calculated for a pure silica fiber in all the simulations, since the change in $A_{eff}(\omega)$ by using the alternative glass compositions was found to be negligible.

The resulting spectra are shown in Fig. 5. The pure silica fibre and the fibre with 1% F both have a ZDW at $\sim$2.6–2.7 μm. It is seen in Fig. 5 that in these fibres the solitons have red-shifted to $\sim$2.5 μm and generate dispersive waves at $\sim$3 μm (when loss is not included). The fibre with

13.3% B_2O_3 has a ZDW at ~2.9 μm, and the solitons have here also red-shifted to ~2.5 μm and generate dispersive waves at ~ 3.1 μm. For the simulations including loss, the dispersive waves are attenuated so much that they are not visible in the spectrum.

At the short-wavelength edge of the spectra, we see that using a fibre with 1% F results in practically the same blue-shift as when using a pure silica fibre. As mentioned in Section 3 this is expected because $v_g(\lambda)$ is upshifted more in the wavelength region of red-shifting solitons (between the pump wavelength and the higher ZDW) than in the visible wavelength region of the dispersive waves. The fibre with 13.3% B_2O_3 has a smaller upshift of $v_g(\lambda)$ in the wavelength region of dispersive waves, but this is more than compensated by the downshift of $v_g(\lambda)$ in the wavelength region of red-shifting solitons (see Fig. 3). This explains why the short-wavelength edge of the spectrum calculated for the 13.3% B_2O_3 fibre is more blue-shifted than in the pure silica fibre.

In Fig. 3 (left) we have also drawn lines between $v_g(\lambda)$ at the short-wavelength edge of the spectrum and the wavelength to which the solitons have red-shifted. These lines are almost horizontal indicating that there is almost perfect group-velocity match between the red-shifting solitons and the blue-shifted dispersive waves (again, we neglect the nonlinear contribution to the group-velocity of a soliton). This again supports the understanding of the physical mechanism behind the blue-shift described in Section 2.

6. Conclusion

In conclusion, this work demonstrates that modifying the group-velocity profile by changing the glass composition of the nonlinear fibre can be used to increase the blue-shift of the supercontinuum. It was found that care must be taken to ensure that the change in glass composition does not just lead to an upshift of the entire group-velocity profile, but that the resulting group-velocity at the long-wavelength part of the spectrum must be lowered relative to the group-velocity at the short-wavelength part of the spectrum. One could also combine a modification of the glass material to raise $v_g(\lambda)$ at short wavelengths, with a modification of the PCF structure to lower $v_g(\lambda)$ at long wavelengths. This is feasible because the material dispersion is dominant for short wavelengths and the waveguide dispersion is dominant for long wavelengths. The combination of designing a suitable group-velocity profile using both an alternative glass composition and an optimized PCF structure, can be expected to lead to an even larger blue-shift of the generated supercontinuum.

We point out that this investigation did not consider how the alternative glass composition could result in a different nonlinearity and/or a different loss, than that obtained in pure silica fibers, and how this could affect the generated supercontinuum. However, n_2 is expected to increase in the alternative glass compositions [43], which increases the efficiency of the nonlinear spectral broadening mechanisms. The loss, however, is also expected to increase, and this could limit the soliton red-shift into the near-infrared, thereby limiting the additional blue-shift that could be expected from the modification of the group-velocity profile alone. Further investigations will therefore have to determine the loss profile of the alternative glass compositions, before we know with certainty whether an additional blue-shift can be obtained through this approach.